COVID-19 Detection in Chest X-ray Images using Deep Learning Approach

Authored by: Manasij Haldar

Chandigarh University, Mohali, Punjab, India

Abstract

The Corona Virus Disease (COVID-19) is a novel virus that has never been seen in humans previously. The virus produces a respiratory infection similar to the flu, with symptoms such as cough and fever that can progress to pneumonia in severe instances. COVID-19 spreads swiftly among humans, impacting around 1,200,000 persons around the world at the time of authoring this report (April 2020). Because the number of contagious diseases and deaths is increasing every day, the goal of this project is to use deep learning techniques to develop a rapid approach for detecting COVID-19 in chest X-ray pictures. An object detection architecture is developed, trained, and evaluated for this purpose using a publicly available dataset of 1500 photos of non-infected and infected individuals with COVID-19 and pneumonia. Our method's major purpose is to determine if a patient's COVID-19 instance is positive or negative. In our studies, we acquire a COVID-19 detection sensitivity of 94.92 percent and specificity of 92.00 percent using the SDD300 model, proving the utility of utilizing deep learning models to classify COVID-19 in X-ray pictures.

Keywords: COVID-19, Deep Learning, Object Detection, X-ray, Convolutional Neural Network (CNN).

INTRODUCTION

Throughout the first months of 2020, the new SARS-CoV-2 coronavirus, which causes COVID-19, had the entire world on edge. It caused many nations' borders to close and millions of inhabitants to be confined to their homes due to sick persons, with 868,000 confirmed cases worldwide at this time (April 2020). In December of this year, the virus was discovered in China. Since March 2020, Europe has been the epicenter of the virus's spread.

China has managed to contain the virus over three months after the outbreak began in December 2019, with a total of 3,312 deaths and more than 81,000 afflicted persons. According to a report released in April 2020, Italy, which overtook the Asian countries in death toll in March 2020, has become the most impacted country, with more than 10,000 people killed. This number was steadily increasing. Various studies projected the expansion of infection curves based on various parameters such as the number of exposed, infected, and recovered humans. These investigations helped researchers to gain a better understanding of the transmission dynamics that may occur in each country.

The outbreak's cause has yet to be determined. The first cases were discovered in December of this year. Respiratory symptoms, fever, cough, dyspnea, and viral pneumonia are all clinical features of COVID-19. The fundamental issue with these symptoms is that there are virus-infected persons who are asymptomatic.

COVID-19 is detected through the collection of samples from the respiratory tract. When the case study is asymptomatic or symptoms are light, it is performed at home by a health care expert, or in a health facility or hospital if the patient is admitted for a serious ailment. In nations like Germany and South Korea, performing as many tests as possible has proven to be the most effective way to combat the virus. Because Spain was unable to conduct so many tests, it is critical to explore and create alternate techniques for doing these tests in a timely and efficient manner.

In the detection and follow-up of disease, AI and radiomics applied to X-Ray and Computed Tomography (CT) are useful tools. According to CT scans, significant ground grass opacity lesions in the peripheral and posterior lungs indicate COVID-19 pneumonia. As a result, once abnormalities in chest radiographs are suggestive of coronavirus, CT can play a crucial role in the diagnosis of COVID-19 as an advanced imaging evidence. AI algorithms and radiomics features generated from chest X-rays would be extremely useful in implementing large-scale screening programmes in any country with X-ray capability, and would aid in the diagnosis of COVID-19.

The current circumstance necessitates the implementation of an automatic detection system as an alternative diagnosis option to stop COVID-19 from spreading. Several researchers have used machine learning to accomplish this goal, such as the Size Aware Random Forest approach (iSARF) proposed by, in which participants were divided into groups with varying sizes of infected lesions. Then, with each group, a random forest-based classifier was trained. Under five-fold cross-validation, their proposed technique generated an accuracy of 0.879, a sensitivity of 0.907, and a specificity of 0.833, according to the results.

In order to produce better outcomes than more typical machine learning approaches, deep learning techniques are also applied. Convolutional neural networks are one of the most widely utilized approaches in picture categorization (CNNs). This type of model has been used in several studies to detect COVID-19 in medical images, such as in, where the authors propose a CNN model trained with a randomly selected set of image regions of interest (ROIs), achieving an accuracy of 85.2 percent, a specificity of 0.83, and a sensitivity of 0.67. Another example of what may be accomplished with CNNs is offered by. They propose the COVID-Net CNN network, which achieves 92.4 percent accuracy, 80% sensitivity, and 88.9% specificity.

COVIDX-Net is a method that combines seven distinct deep convolutional neural network designs, including a modified version of the Visual Geometry Group Network (VGG19) and the second edition of Google MobileNet. Each deep neural network model can categorize the patient's status as a

negative or positive COVID-19 case by analyzing the normalized intensities of the X-ray image. For healthy and COVID-19 detection, their trials reach f1-scores of 0.89 and 0.91, respectively.

The findings in the cited papers suggest that deep learning techniques are beneficial for virus identification and that they improve the metrics acquired using more typical machine learning methods.

Our paper's main contribution is to increase COVID-19 detection accuracy by offering a new dataset that combines COVID-19 and pneumonia images to create more consistent predictions and by using image processing to allow image normalization and improve model learning.

PROBLEM DEFINITION

The reference diagnostic test for COVID-19 pneumonia is real-time reverse transcription-polymerase chain reaction (RT-PCR). The specificity of RT-PCR is approximately 95%, but the sensitivity of RT-PCR at the initial presentation is 60–71% because of kit performance, sampling and transportation limitations. Because of these low sensitivity rates and the need for rapid diagnosis, X-Ray has been frequently used in the current pandemic condition. Also, several cases with initial negative RT-PCR results are reported to have positive chest CT findings or X-rays. So in the direction of finding an accurate way of testing Covid19, X-rays tend to be more trustworthy than any RT-PCR reports, blood reports or various other symptoms. Which led us here for the project of Covid19 Detection analyzing X-Ray imagery using Neural Networks.

PROBLEM FORMULATION

Background

During a pandemic, such as COVID-19, a timely and precise diagnosis is critical. It improves patient outcomes and relieves burden on health-care systems that are dealing with a growing rate of infection.
The polymerase chain reaction (PCR) is the current preferred approach for diagnosing COVID-19 (PCR). However, some of the worst-affected locations are unable to obtain enough kits to fulfill demand, and many countries are unable to conduct tests due to a lack of lab facilities.
Deep learning models, which are a type of artificial intelligence (AI), are being studied and used to detect and diagnose a wide range of diseases.

Deep learning algorithms could be employed in this case to identify infected individuals using chest X-ray scans, which are readily available around the world. This approach could be employed in situations where PCR diagnostics are currently unavailable.
Deep learning for X-ray analysis might drastically cut the time it takes to diagnose patients, with an AI model processing up to 200 images in the time it takes a radiologist to analyze one.

Method

We propose using a deep convolutional neural network trained on COVID-19 and pneumonia images, as well as a fresh dataset comprising COVID-19 and pneumonia images. Both are open to the public via GitHub and Kaggle, respectively. COVID-19 cases are represented by the chest X-ray or CT images available on GitHub. It was made by putting together medical photos from publicly accessible sources and publications. There are 204 COVID-19 X-ray pictures in this dataset. The Kaggle dataset, on the other hand, was produced for a pneumonia detection challenge. Bounding boxes surround sick lung regions in the photos. Without the boundary boxes, the samples are negative and show no signs of pneumonia. The presence of bounding boxes in samples indicates the presence of pneumonia.
By combining COVID-19 and pneumonia images, we propose a new dataset that is both larger and more diversified. Because normal pneumonia and COVID-19 have comparable appearances in chest X-ray images, including pneumonia images in the training dataset implies an extra advantage. This dataset merger enables the creation of a more robust model capable of distinguishing between those diseases. Another benefit of this merge is that it expands the train dataset, which is important because COVID-19 photos are scarce at the time of authoring this research. Because of the similarities between pneumonia and COVID-19, this merge does not increase the size of the COVID-19 picture collection, but it does improve detection quality.

To avoid biased findings, we split the photos into train and test sets, dividing all the data in a balanced way, meaning that all samples of each class in the training sets are well-balanced. Despite the fact that we have a significant number of pneumonia and normal photos, we created a dataset of 1500 photographs for this reason.
For training, we chose 104 COVID-19 images, 205 health lung images, and 204 pneumonia images, and for testing, we chose 100 COVID-19 images, 444 health lung images, and 443 pneumonia images. There are more samples of pneumonia and normal photos in the Kaggle dataset, but we chose only 205 for training to ensure a balanced dataset. We add more pneumonia and normal photos to the test stage to demonstrate the model's robustness in detecting COVID-19 with no false positives. To summarize, we employ a total of 513 photos in the train set and 887 images in the test set.

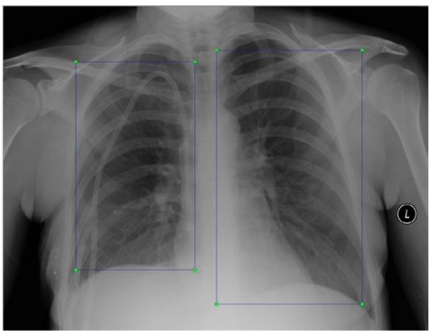

LITERATURE REVIEW

CXRs are a good monitor of COVID-19 chest manifestations and its scoring system provides an accurate method to predict the disease severity. The study also revealed a positive correlation between the patients' age and total severity score to the final disease outcome providing a good indicator for

clinician to identify at an early stage the patients with the highest risk and plan specific treatment strategies for them.

COVID-19 is a highly infectious disease that has been spread widely throughout the world. The disease management strategies primarily depend upon the early disease diagnosis. However, the dramatic dissemination of the disease created a great challenge due to the insufficient laboratory kits . That is why radiology has become a forefront method during the outbreak of COVID-19 .

Current literature is mostly assessing COVID-19 CT findings, as it offers more sensitive results than chest X-ray (CXR) especially in the initial assessment of the patients. The increased number of hospitalized patients and the consequent increase in radiological examinations would make the constant use of chest CT scan (from diagnosis to discharge) difficult to sustain over time . The dependence on CT creates a huge burden on radiology departments and this makes the CXRs greatly substitute the CT examinations . Although chest X-ray (CXR) is considered less sensitive for the detection of pulmonary involvement in early-stage disease, it is useful for monitoring the rapid progression of lung abnormalities in COVID-19, especially in critical patients admitted to intensive care units . To provide valuable help for the clinicians and improve the stratification of the disease risk, chest X-ray (CXR) scoring system was tailored providing a semi-quantitative tool for assessment of lung abnormalities .

In this study, we analyzed the CXRs findings and severity scores of patients proven to have COVID-19 in dif erent stages of disease. CXRs abnormalities were detected in 268 of 350 patients (77%) at certain points of the disease course. In our study, each lung was given a score of 0–4 depending on the extent of lung involvement (score 0 = no involvement; 1 ≤ 25%; 2 = 25–50%; 3 = 50–75%; 4 ≥ 75% lung af ection). A total severity score was calculated by summing both lung scores (total severity scores ranged from 0 to 8). Borghesi et al. made another CXR scoring system for COVID-19 pneumonia (Brixia score) by dividing the lungs to six zones on frontal projection (upper, middle, and lower zones); then, a score (from 0 to 3) is assigned to each zone based on the lung abnormalities detected on frontal chest projection as follows: score 0, no lung abnormalities; score 1, interstitial infiltrates; score 2, interstitial and alveolar infiltrates (interstitial predominance); and score 3, interstitial and alveolar infiltrates (alveolar predominance). The scores of the six lung zones are then added to obtain an overall "CXR SCORE" ranging from 0 to 18 . In our study, most of the patients showed bilateral lung af ection (181 patients, 67.5%) with lower zonal predominance (196, 73.1%) and peripheral distribution (156 patients, 58.2%) . The most common CXRs features detected in COVID-19 cases were consolidation seen in 218 patients (81.3%), followed by reticular interstitial thickening seen in 107 patients (39.9%) and GGO seen in 87 patients (32.5%). Few cases showed pulmonary nodules seen in 25 patients (9.3%) and pleural ef usion seen in 20 patients (7.5%). This agreed with Wong et al. who did a study on 64 COVID-19 patients, they found that Consolidation was the most common finding (47%), followed by GGO (33%). Also, peripheral predominance was seen in 41% of CXR abnormalities with lower zone distribution (50%) with bilateral lung involvement (50%). Pleural effusion was uncommon, only seen in 3% . Also, Lomoro et al. performed a study on thirty-two patients of COVID-19 disease; they found that consolidation is the most common finding (46.9%) with bilateral lung infection in (78.1%) and lower zone involvement (52%). No pleural effusion was identified . Jacobi et al. stated that standard CXR can easily identify reticular opacities accompanying regions of ground glass attenuation. They state that air space consolidation opacities with peripheral and lower zone distribution are unique for COVID-19 disease . Chen et al. reported bilateral pneumonia as the most common finding on chest radiographs . While, Ng et al. reported that CXR lacks sensitivity in the early stages of lung disease . In most studies, pleural effusions, pneumothorax, and lung cavitation are rare in COVID-19 infected patients . Pneumothorax was detected in 2 cases in our study and it was iatrogenic due to mechanical ventilation in intubated patients. We classified patients according to the stage of illness into four stages (1–4 days, 5–9 days, 10–15 days, and > 15 days). The degree of disease severity was assessed using a semi-quantitative CXRs severity score that reflects the severity of different stages of this disease. The total severity score was lowest at stage 1 compared to other stages, with significant difference among other stages, indicating that the disease changed rapidly within 10–15 days after the onset of the initial symptoms. We estimated the total severity score in the baseline and follow-up CXR, and it ranged from 0 to 8. In most cases (230 patients, 65.7%), TSS was mild, ranging between 0 and 2. While, in 82 patients (23.4%), there was a moderate severity score ranging between 3 and 5. Severe cases with a severity score of between 6 and 8 was found in 38 patients (10.9%) with more disseminated lung involvement. Wong et al. found in their study that 41% had mild findings with a total severity score of 1–2, while moderate and severe cases with more extensive lung involvement were seen in 20% and 8% patients, who had severity scores of 3–4 and 5–6, respectively. There was no patient who had a severity score of > 6 on their baseline CXR with the severity of CXR findings peaking at 10–15 days from the date of symptom onset . In our study, the maximum total severity score was reached in 113 patients (42.2%) in the initial baseline CXR with mean total severity score 1.49 ± 1.53 followed by 92 patients (34.3%) who reached the maximum TSS at 1st follow-up CXR done (done 1–4 days) with mean total severity score 2.08 ± 1.83. The highest total severity score of the CXR findings was found in the 4th follow-up CXR 15 days after the onset of the symptoms with its mean 4.51 ± 1.61. Our study correlated the disease outcome to the patients' age with a significant difference between the age of the patients and COVID-19 disease outcome (P value = 0.008). The mean age for the recovered patients was 41.09 ± 14.14 while the mean age for the dead patients was 51.04 ± 10.17. Lowest mortality rate was observed in 20–40 years, while patients aging 40–59 and ≥ 60 years showed significantly higher mortality rate. In our study, there were 261 males (74.6%) and 89 females (25.4%) with male patients showing significantly higher mortality rate compared to the female patients (P value 0.025). This agreed with Borghesi et al., who did a study on 783 Italian patients. They found that most patients (67.9%) were males and only 15.2% were younger than 50 years. They stated that in older

age groups between 50 and 79 years, there was more significant pulmonary infection with highest severity score seen in males ≥ 50 years or female ≥ 80 especially that underlying comorbidities (such as hypertension, diabetes, cardiovascular disease, and oncologic history) are risk factors of fatal outcome in adult patients with confirmed SARS-CoV-2 infection . In our study, the disease outcome showed a positive correlation with the maximum severity score (6.87 ± 0.71 for the dead patients and 2.06 ± 1.84 for the surviving patients) with high statistical significance (P value < 0.001). In patients with TSS 2, there was a statistical significance between the TSS and the outcome of COVID disease for the survived patients (P value 0.032), while, in patients with TSS 7 and 8, there was a highly statistical significance for the outcome for the dead patients (P value < 0.001). This agreed with Toussie et al. that showed that the severity of lung involvement on the initial chest radiograph was associated with more need for patients' hospitalization as well as the increased risk of intubation and have proposed the use of initial CXR severity scores as a prognostic indicator of COVID-19 patients' outcome. The major strength of this study is the large sample size, which consisted of 350 COVID-19 patients. Our study had some limitations. First, it is a retrospective analysis. Second, the lack of correlation between CXR severity score and patient comorbidities (such as hypertension, diabetes, cardiovascular disease, and oncologic history). Third, not all the patients could be followed till the final outcome as the course of the disease was truncated in these patients. Fourth, CXR serial follow-up studies were not performed in a uniform pattern as it was dedicated by the clinician as regards the clinical condition. Fifth, for severe cases in the intensive care unit, the portable AP CXR was suboptimal with only few cases performed CT, so we could not judge the sensitivity of CXR

MODEL ARCHITECTURE

The employed architecture was chosen based on the good results gained with CNNs in state-of-the-art works for COVID-19 image classification, as well as the good results obtained with this kind of architecture in other related tasks. Based on the Single Shot Multibox Detector, we adopted the same network design provided in (SSD). Using a single deep neural network, this design is optimized for recognising objects in photos. This method divides the output space of bounding boxes into a series of default boxes for each feature map point, using varying aspect ratios and sizes. The network generates scores for the presence of each item type in each default box at prediction time, and then adjusts the box to better match the object shape.

SSD offers comparable accuracy to approaches that use more than one architecture for detecting objects, while being faster and providing a single framework for both training and inference, according to experimental results on various notable datasets. SSD offers substantially better accuracy than other single-stage algorithms, even with a smaller input image size.

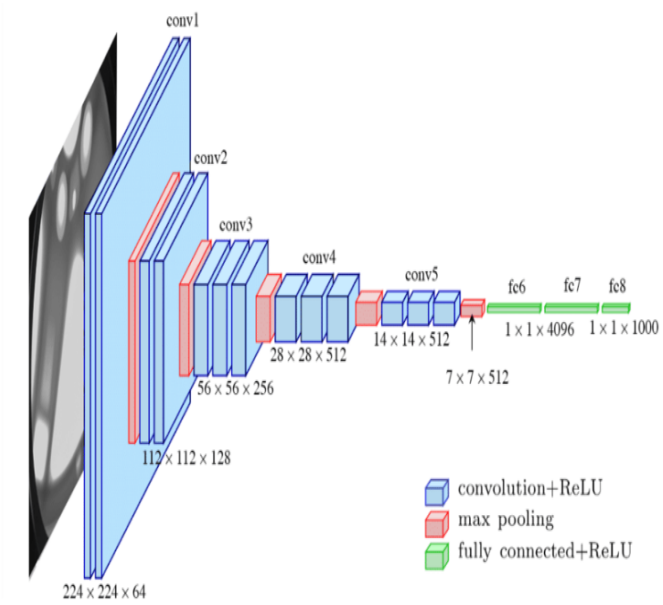

In this design, we employ VGG-16 as the basis network for feature extraction. Fast R-CNN is also used in this model. We have many boxes with varied sizes and aspect ratios over the entire image during training. When compared to the ground truth, SSD determines the box with the highest Intersection-Over-Union (IoU).

Our main goal is to develop a more robust model that can handle a wide range of input item sizes and forms. As a result, a data augmentation step is conducted during the SSD training. The following operations are applied to each image in the dataset as part of this process:

• Keep the original input image in its entirety.
• Pick a patch with a minimum overlap of 0.1, 0.3, 0.5, 0.7, or 0.9 with the objects. Each sampled patch is a proportion of the original image size between [0.1, 1].
• Pick a patch at random.

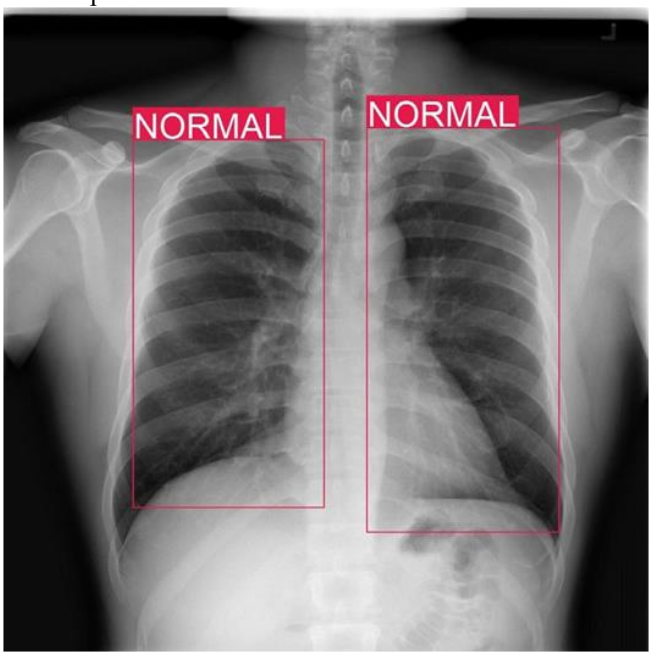

MODEL COMPARISON REVIEW

Before finalizing the Model with VGG-16, a few other models were also trained and tested with the same dataset for a comparative study on the accuracy on each of them.
For the study, the following pre-built models were used from the keras.applications library:

- DenseNet169
- VGG16
- InceptionV3
- ResNet152V2

Details on the models are provided for a better idea.

1. DENSENET169

DenseNet was developed specifically to improve the declined accuracy caused by the vanishing gradient in high-level neural networks. In simpler terms, due to the longer path between the input layer and the output layer, the information vanishes before reaching its destination. An output of the previous layer acts as an input of the second layer by using *composite function operation.* This composite operation consists of the convolution layer, pooling layer, batch normalization, and non-linear activation layer. It is a convolutional neural network where each layer is connected to all other layers that are deeper in the network. To preserve the feed-forward nature, each layer obtains inputs from all the previous layers and passes on its own feature maps to all the layers which will come after it. Unlike Resnets it does not combine features through summation but combines the features by concatenating them. This introduces '(L*(L+1)) connections' rather than just 'L' connections as in traditional deep learning architectures.

The layer architecture of DenseNet169 is given as:

Layers	Output Size	DenseNet 169
Convolution	112×112	7×7 conv, stride 2
Pooling	56×56	3×3 max pool, stride 2
Dense Block (1)	56×56	$\begin{bmatrix} 1 \times 1 \text{ conv} \\ 3 \times 3 \text{ conv} \end{bmatrix} \times 6$
Transition Layer (1)	56×56	1×1 conv
	28×28	2×2 average pool, stride 2
Dense Block (2)	28×28	$\begin{bmatrix} 1 \times 1 \text{ conv} \\ 3 \times 3 \text{ conv} \end{bmatrix} \times 12$
Transition Layer (2)	28×28	1×1 conv
	14×14	2×2 average pool, stride 2
Dense Block (3)	14×14	$\begin{bmatrix} 1 \times 1 \text{ conv} \\ 3 \times 3 \text{ conv} \end{bmatrix} \times 32$
Transition Layer (3)	14×14	1×1 conv
	7×7	2×2 average pool, stride 2
Dense Block (4)	7×7	$\begin{bmatrix} 1 \times 1 \text{ conv} \\ 3 \times 3 \text{ conv} \end{bmatrix} \times 32$
Classification Layer	1×1	7×7 global average pool
	1000	1000D fully-connected, softmax

2. VGG16

VGG16 is a convolution neural network (CNN) architecture that was awarded first place in the 2014 ILSVR (Imagenet) competition. It is widely recognised as one of the best vision model designs available today. Instead of a large number of hyper-parameters, VGG16 focuses on having convolution layers of 3x3 filter with stride 1 and always uses the same padding and maxpool layer of 2x2 filter with stride 2. This layout of convolution and max pool layers is maintained throughout the architecture. Finally, for output, it has two FC (fully connected layers) and a softmax. The number 16 in VGG16 alludes to the fact that it contains 16 weighted layers. This network is quite large, with an estimated 138 million parameters.
The layer architecture of VGG16 is given as:

Layer		Feature Map	Size	Kernel Size	Stride	Activation
Input	Image	1	224 x 224 x 3	-	-	-
1	2 X Convolution	64	224 x 224 x 64	3x3	1	relu
	Max Pooling	64	112 x 112 x 64	3x3	2	relu
3	2 X Convolution	128	112 x 112 x 128	3x3	1	relu
	Max Pooling	128	56 x 56 x 128	3x3	2	relu
5	2 X Convolution	256	56 x 56 x 256	3x3	1	relu
	Max Pooling	256	28 x 28 x 256	3x3	2	relu
7	3 X Convolution	512	28 x 28 x 512	3x3	1	relu
	Max Pooling	512	14 x 14 x 512	3x3	2	relu
10	3 X Convolution	512	14 x 14 x 512	3x3	1	relu
	Max Pooling	512	7 x 7 x 512	3x3	2	relu
13	FC	-	25088	-	-	relu
14	FC	-	4096	-	-	relu
15	FC	-	4096	-	-	relu
Output	FC	-	1000	-	-	Softmax

3. INCEPTIONV3

The Inception V3 is a deep learning model for image categorization that is based on Convolutional Neural Networks. The Inception V3 is an improved version of the fundamental model Inception V1, which was introduced in 2014 as GoogLeNet. It was created by a Google team, as the name implies. It has a total of 42 layers and a lower error rate than its predecessors.

The components the InceptionV3 model is made of are:

TYPE	PATCH / STRIDE SIZE	INPUT SIZE
Conv	3×3/2	299×299×3
Conv	3×3/1	149×149×32
Conv padded	3×3/1	147×147×32
Pool	3×3/2	147×147×64
Conv	3×3/1	73×73×64
Conv	3×3/2	71×71×80
Conv	3×3/1	35×35×192
3 × Inception	Module 1	35×35×288
5 × Inception	Module 2	17×17×768
2 × Inception	Module 3	8×8×1280
Pool	8 × 8	8 × 8 × 2048
Linear	Logits	1 × 1 × 2048
Softmax	Classifier	1 × 1 × 1000

RESNET152V2

Residual Network (ResNet) is a Convolutional Neural Network (CNN) design that addresses the "vanishing gradient" problem, allowing networks with thousands of convolutional layers to outperform shallower networks. During backpropagation, a diminishing gradient occurs. When the neural network training algorithm tries to discover weights that minimize the loss function, if there are too many layers, the gradient becomes very small until it disappears, and optimization is halted. ResNet fixed the issue by utilizing "identity shortcut connections." It works in two stages:

1. ResNet builds and skips numerous levels that are initially not used, recycling activation functions from prior layers.
2. The network is re-trained in a second stage, and the "residual" convolutional layers are extended. This allows for the exploration of extra areas of the feature space that would have been missed by a shallow convolutional network architecture.

The components the ResNet152V2 model is made of are:

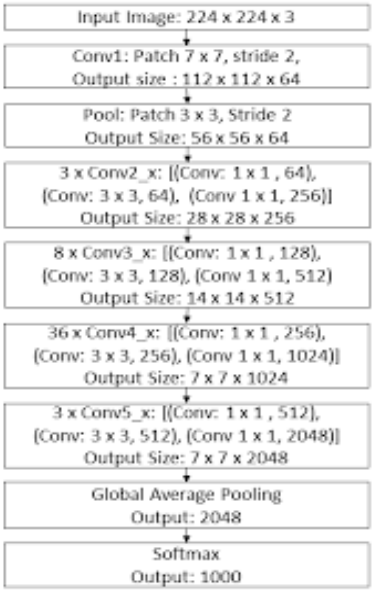

While training the various models, it is seen that the VGG16 model surpasses all the other models for having a better overall performance on the given number of epochs as well as a lesser loss and validation loss rate overall. The comparative study outcome is provided.

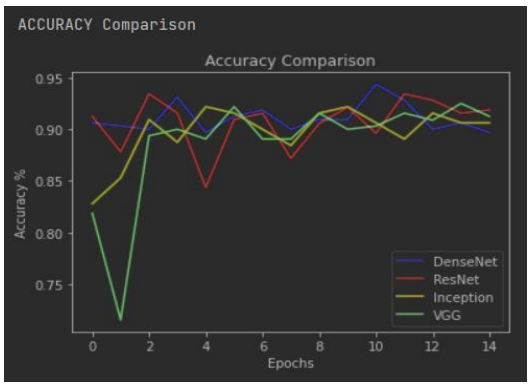

Accuracy

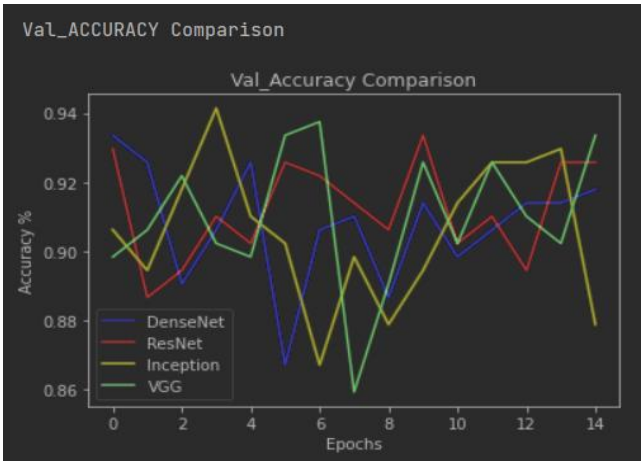

Validation Accuracy

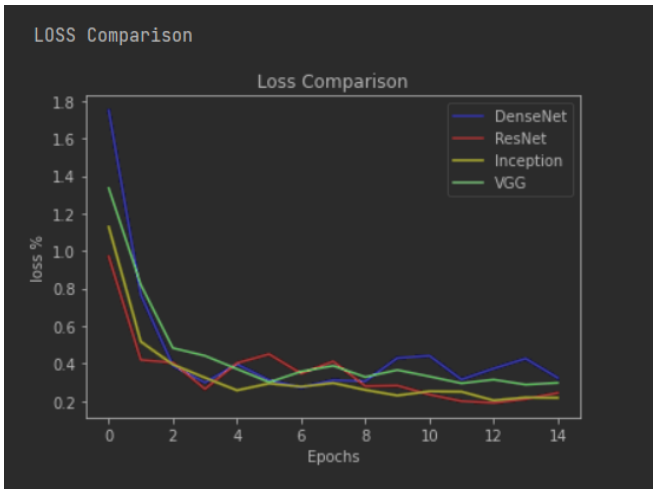

Loss

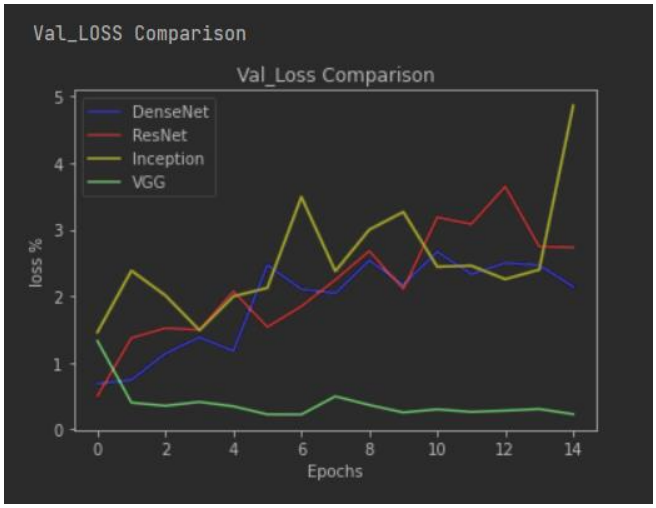

Validation Loss

From the comparison plots of the 4 CNN Models, it can be inferred that even though the other models showed almost similar performance in the overall, but while it comes to Validation Loss, only VGG16 gave a consistent lower rate of loss while the other Models namely Inception, ResNet and DenseNet gave out an increasing rate of losses with visible fluctuations.

EXPERIMENTATION RESULT

The contrast modification of each image in the dataset is the first experiment conducted in this study. Because the exposure time of X-Ray images might vary between acquisitions, this adjustment is required. Because the dataset's photos come from many hospitals around the world, each location's image acquisition settings and conditions are unique. A change in the voltage spike results in a change in the contrast of the radiography in X-Ray images. Exposure duration, or the amount of time that x-rays are created, is another component that impacts the contrast of the image obtained.

```
The given X-Ray image is of type = Covid

The chances of image being Covid is : 54.84541058540344
The chances of image being Normal is : 26.9942402839660

image with heatmap representing the covid spot
```

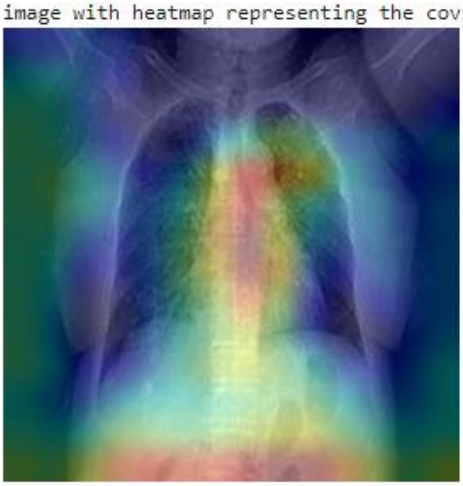

Contrast Limited Adaptive Histogram Equalization (CLAHE) is used to achieve image similarity throughout the dataset.

This is a transformation that seeks to give a picture a histogram with a uniform distribution. That is, each level of grey in a monochrome image's histogram has the same amount of pixels. According to, when continuous exposure is utilized in X-ray imaging to generate an image sequence or video, low-level exposure is frequently used until the region of interest is determined, limiting the amount of radiation applied to the patients.

```
The given X-Ray image is of type = Normal

The chances of image being Covid is : 22.541259229183197 %
The chances of image being Normal is : 66.90725088119507 %

image with heatmap representing the covid spot
```

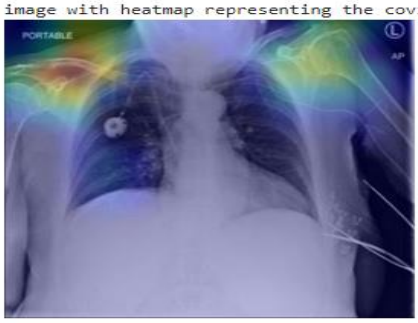

Images with a low signal-to-noise ratio are obtained as a disadvantage. In this example, as well as many others, it is beneficial to increase image quality by employing image enhancing techniques such as histogram equalization methods

We use ImageNet-trained VGG-16 weights to load. Many studies, particularly in small datasets , have examined the accuracy gain achieved by transfer learning. We employ these weights because, despite the fact that lower layers learn features that aren't necessarily unique to this dataset, this step enhances detection accuracy, as well as the sensibility and specificity measures. The fundamental concept is to use a trained model for similar images and adapt a base-learner to a new task with few labelled examples.

CONCLUSION

This research shows how image pre-processing and the proposed object detection model can be used to detect COVID-19 in chest X-ray pictures.
The suggested integrated dataset with pneumonia images enables for the development of a more robust model that can differentiate between COVID-19 and pneumonia disorders. We can generate a normalized dataset using the histogram equalization technique, which helps us model the training step. It also enhances normal picture detection while lowering the probability of false positives.
These findings show that object detection models trained with additional photos of similar diseases and using transfer learning, in combination with the CLAHE algorithm for image normalization, can be effective in medical decision-making procedures including the COVID-19 viral diagnosis.

REFERENCES

1. M. Dur-e-Ahmad and M. Imran, “Transmission Dynamics Model of Coronavirus COVID-19 for the Outbreak in Most Affected Countries of the World,” International Journal of Interactive Multimedia and Artificial Intelligence, vol. In Press, no. In Press, pp. 1-4, 2020.

2. S. J. Fong, N. D. G. Li, R. Gonzalez-Crespo and E. Herrera-Viedma, “Finding an Accurate Early Forecasting Model from Small Dataset: A Case of 2019-nCoV Novel Coronavirus Outbreak,” International Journal of Interactive Multimedia and Artificial Intelligence, vol. 6, no. 1, pp. 132- 140, 2020.

3. Q. Li, X. Guan, P. Wu, X. Wang, L. Zhou, Y. Tong, R. Ren, K. S. M. Leung, E.H.Y. Lau, J. Y. Wong and others, “Early transmission dynamics in Wuhan, China, of novel coronavirus–infected pneumonia,” New England Journal of Medicine, 2020.

4. D. Wang, B. Hu, C. Hu, F. Zhu, X. Liu, J. Zhang, B. Wang, H. Xiang, Z. Cheng, Y. Xiong, Y. Zhao, Y. Li, X. Wang and Z. Peng, "Clinical Characteristics of 138 Hospitalized Patients With 2019 Novel Coronavirus–Infected Pneumonia in Wuhan, China," JAMA, vol. 323, pp. 1061-1069, 3 2020.

5. S. Chauvie, A. De Maggi, I. Baralis, F. Dalmasso, P. Berchialla, R. Priotto, P. Violino, F. Mazza, G. Melloni and M. Grosso, "Artificial intelligence and radiomics enhance the positive predictive value of digital chest tomosynthesis for lung cancer detection within SOS clinical trials," European Radiology, p. 1–7, 2020.

6. G. Chassagnon, M. Vakalopoulou, N. Paragios and M.-P. Revel, "Artificial intelligence applications for thoracic imaging," European Journal of Radiology, vol. 123, p. 108774, 2020.

7. F. Song, N. Shi, F. Shan, Z. Zhang, J. Shen, H. Lu, Y. Ling, Y. Jiang and Y. Shi, "Emerging 2019 Novel Coronavirus (2019-nCoV) Pneumonia," Radiology, vol. 295, pp. 210-217, 2020.

8. J. C. L. Rodrigues, S. S. Hare, A. Edey, A. Devaraj, J. Jacob, A. Johnstone, R. McStay, A. Nair and G. Robinson, "An update on COVID-19 for the radiologist-A British society of Thoracic Imaging statement," Clinical Radiology, 2020.

9. J. Wu, J. Liu, X. Zhao, C. Liu, W. Wang, D. Wang, W. Xu, C. Zhang, J. Yu, B. Jiang and others, "Clinical characteristics of imported cases of COVID-19 in Jiangsu province a multicenter descriptive study," Clinical Infectious Diseases, 2020.

10. F. Shi, L. Xia, F. Shan, D. Wu, Y. Wei, H. Yuan, H. Jiang, Y. Gao, H. Sui and D. Shen, Large-Scale Screening of COVID-19 from Community Acquired Pneumonia using Infection Size-Aware Classification, arXiv preprint arXiv:2003.09860, 2020.

11. S. Wang, J. M. Bo Kang, X. Zeng and M. Xiao, "A deep learning algorithm using CT images to screen for Corona Virus Disease COVID-19)," medRxiv, 2020.

12. L. Wang and A. Wong COVID-Net A Tailored Deep Convolutional Neural Network Design for Detection of COVID-19 Cases from Chest Radiography Images, arXiv preprint arXiv:2003.09871 ,2020.

13. E. E.-D. Hemdan, M. A. Shouman and M. E. Karar, COVIDX-Net A Framework of Deep Learning Classifiers to Diagnose COVID-19 in X-Ray Images, arXiv preprint arXiv: arXiv:2003.11055, 2020.

14. J. P. Cohen, P. Morrison and L. Dao, COVID-19 Image Data Collection, arXiv preprint arXiv: arXiv, arXiv:2003.11597, 2020.

15. RSNA Pneumonia Detection Challenge. Kaggle. [online] Available at: https://www.kaggle.com/c/rsna-pneumonia-detection-challenge, Accessed 29 April 2020.

16. M. Everingham, L. Van Gool, C. K. I. Williams, J. Winn and A. Zisserman, "The pascal visual object classes (voc) challenge," International journal of computer vision, vol. 88, p. 303–338, 2010.

17. W.Liu, D. Anguelov, D. Erhan, C. Szegedy, S. Reed, C.-Y. Fu and A. C. Berg, "SSD Single Shot MultiBox Detector," Lecture Notes in Computer Science, p. 21–37, 2016.

18. K.Simonyan and A. Zisserman, "Very Deep Convolutional Networks for Large-Scale Image Recognition," CoRR, vol. abs1409.1556, 2014.

19. H. Jansen, Radiología dental. Principios y técnicas., Mc Graw Hill, 2002.

20. A. M. Reza, "Realization of the contrast limited adaptive histogram equalization (CLAHE) for real-time image enhancement," Journal of VLSI signal processing systems for signal, image and video technology, vol. 38, p. 35–44, 2004.

21. H.-W. Ng, V. D. Nguyen, V. Vonikakis and S. Winkler, "Deep learning for emotion recognition on small datasets using transfer learning," in Proceedings of the 2015 ACM on international conference on multimodal interaction, 2015.

22. Q. Sun, Y. Liu, T.-S. Chua and B. Schiele, "Meta-transfer learning for few-shot learning," in Proceedings of the IEEE Conference on Computer Vision and Pattern Recognition, 2019.